Research Article

Four-Neutrino Analysis of 1.5 km Baseline Reactor Antineutrino Oscillations

Sin Kyu Kang,[1,2] Yeong-Duk Kim,[3] Young-Ju Ko,[4] and Kim Siyeon[4]

[1] *School of Liberal Arts, Seoul National University of Science and Technology, Seoul 139-743, Republic of Korea*
[2] *Pittsburgh Particle Physics, Astrophysics, and Cosmology Center, Department of Physics and Astronomy,*
University of Pittsburgh, Pittsburgh, PA 15260, USA
[3] *Department of Physics, Sejong University, Seoul 143-747, Republic of Korea*
[4] *Department of Physics, Chung-Ang University, Seoul 156-756, Republic of Korea*

Correspondence should be addressed to Kim Siyeon; siyeon@cau.ac.kr

The masses of sterile neutrinos are not yet known, and depending on the orders of magnitudes, their existence may explain reactor anomalies or the spectral shape of reactor neutrino events at 1.5 km baseline detector. Here, we present four-neutrino analysis of the results announced by RENO and Daya Bay, which performed the definitive measurements of θ_{13} based on the disappearance of reactor antineutrinos at km order baselines. Our results using 3 + 1 scheme include the exclusion curve of Δm_{41}^2 versus θ_{14} and the adjustment of θ_{13} due to correlation with θ_{14}. The value of θ_{13} obtained by RENO and Daya Bay with a three-neutrino oscillation analysis is included in the 1σ interval of θ_{13} allowed by our four-neutrino analysis.

1. Introduction

Understanding of the Pontecorvo-Maki-Nakagawa-Sakata (PMNS) matrix [1] is now moving to another stage, due to the determination of the last angle by multidetector observation of reactor neutrinos at Daya Bay [2] and RENO [3], whose success was strongly expected from a series of oscillation experiments, (T2K [4], MINOS [5], and Double Chooz [6, 7]), which all contributed to the forefront of neutrino physics [8]. A number of 3ν global analyses [9, 10] have presented the best fit and the allowed ranges of masses and mixing parameters at 90% confidence level (CL) by crediting RENO and Daya Bay for the definitive measurements of $\sin^2 2\theta_{13}$. For instance, the best-fit values given in the analysis of Fogli et al. [9] are $\Delta m_{21}^2 = 7.5 \times 10^{-5}$ eV^2, $\sin^2\theta_{12} = 3.2 \times 10^{-1}$, $\Delta m_{32}^2 = 2.4 \times 10^{-3}$ eV^2, $\sin^2\theta_{13} = 2.8 \times 10^{-2}$, and $\sin^2\theta_{23} = 4.8 \times 10^{-1}$ for normal hierarchy. While all three mixing angles are now known to be different from zero, the values of the CP violating phases are completely unknown. Although there are a number of global analysis which presented consistent values

of masses and mixing parameters [9–11], we focus on θ_{13} and its associated factors obtained by RENO and Daya Bay.

Although the three-neutrino framework is well established phenomenologically, we do not rule out the existence of new kinds of neutrinos, which are inactive so-called sterile neutrinos. Over the past several years, the anomalies observed in LSND [12], MiniBooNE [13–15], Gallium solar neutrino experiments [16, 17], and some reactor experiments [18] have been partly reconciled by the oscillations between active and sterile neutrinos. In a previous work, we also examined whether the oscillation between sterile neutrinos and active neutrinos is plausible, especially when analyzing the first results released from Daya Bay and RENO [19]. There are also other works with similar motivations [20–25].

After realizing the impact of the large size of θ_{13}, both reactor neutrino experiments have continued and updated the far-to-near ratios and $\sin^2 2\theta_{13}$. Daya Bay improved their measurements and explained the details of the analysis. RENO announced an update with an extension until October 2012 and modified their results as follows. The ratio of the observed to the expected number of neutrino events at the far

detector $R = 0.929$ replaced the former value of $R = 0.920$, and $\sin^2 2\theta_{13} = 0.100$ replaced the former best fit of $\sin^2 2\theta_{13} = 0.113$ [26]. The spectral shape was also modified. Again, we examine the oscillation between a sterile neutrino and active neutrinos in order to determine whether four-neutrino oscillations are preferred to three-neutrino oscillations. This work is focused on Δm_{14}^2 within the range of $\mathcal{O}\left(0.001\ \text{eV}^2\right)$ to $\mathcal{O}\left(0.1\ \text{eV}^2\right)$, where Δm_{14}^2 oscillations might have appeared in the superposition with Δm_{13}^2 oscillations at far detectors of $\mathcal{O}\left(1.5\ \text{km}\right)$ baselines. Since the mass of the fourth neutrino is unknown, it is worth verifying its existence at all available orders of magnitude which are accessible from different baseline sizes. For instance, the near detector at RENO can search reactor antineutrino anomalies with $\Delta m_{14}^2 \sim \mathcal{O}\left(1\ \text{eV}^2\right)$ [27, 28].

This paper is organized as follows. In Section 2, the survival probability of electron antineutrinos is presented in four-neutrino oscillation scheme. We exhibit the dependence of the oscillating aspects on the order of Δm_{21}^2, when reactor neutrinos in the energy range of 1.8 to 8 MeV are detected after travel along a km order baseline. In Section 3, the curves of the four-neutrino oscillations are compared with the spectral shape of data through October 2012 to search for any clues of sterile neutrinos and to see the changes in $\sin^2 2\theta_{13}$ due to the coexistence with sterile neutrinos. Broad ranges of Δm_{41}^2 and $\sin^2 2\theta_{14}$ remain. In the conclusion, the exclusion bounds of $\sin^2 2\theta_{14}$ and the best fit of $\sin^2 2\theta_{13}$ are summarized, and the consistency between rate-only analysis and shape analysis is discussed.

2. Four-Neutrino Analysis of Event Rates in Multidetectors

The four-neutrino extension of unitary transformations from mass basis to flavor basis is given in terms of six angles and three Dirac phases:

$$\widetilde{U}_{\text{F}} = R_{34}\left(\theta_{34}\right) R_{24}\left(\theta_{24}, \delta_2\right) R_{14}\left(\theta_{14}\right) \cdot R_{23}\left(\theta_{23}\right) R_{13}\left(\theta_{13}, \delta_1\right) R_{12}\left(\theta_{12}, \delta_3\right), \tag{1}$$

where $R_{ij}(\theta_{ij})$ denotes the rotation of the ij block by an angle of θ_{ij}. When a 3 + 1 model is assumed as the minimal extension, the 4-by-4 $\widetilde{U}_{\text{F}}$ is given by

$$\widetilde{U}_{\text{F}} = \begin{pmatrix} c_{14} & 0 & 0 & s_{14} \\ -s_{14}s_{24} & c_{24} & 0 & c_{14}s_{24} \\ -c_{24}s_{14}s_{34} & -s_{24}s_{34} & c_{34} & c_{14}c_{24}s_{34} \\ -c_{24}c_{34}s_{14} & -s_{24}c_{34} & -s_{34} & c_{14}c_{24}c_{34} \end{pmatrix}$$

$$\times \begin{pmatrix} U_{e1} & U_{e2} & U_{e3} & 0 \\ U_{\mu 1} & U_{\mu 2} & U_{\mu 3} & 0 \\ U_{\tau 1} & U_{\tau 2} & U_{\tau 3} & 0 \\ 0 & 0 & 0 & 1 \end{pmatrix} \tag{2}$$

$$= \begin{pmatrix} c_{14}U_{e1} & c_{14}U_{e2} & c_{14}U_{e3} & s_{14} \\ \cdots & \cdots & \cdots & c_{14}s_{24} \\ \cdots & \cdots & \cdots & c_{14}c_{24}s_{34} \\ \cdots & \cdots & \cdots & c_{14}c_{24}c_{34} \end{pmatrix},$$

where the PMNS type of a 3-by-3 matrix U_{PMNS} with three rows, $(U_{e1}\ U_{e2}\ U_{e3})$, $(U_{\mu 1}\ U_{\mu 2}\ U_{\mu 3})$, and $(U_{\tau 1}\ U_{\tau 2}\ U_{\tau 3})$, is imbedded. The CP phases δ_2 and δ_3 introduced in (1) are omitted for simplicity, since they do not affect the electron antineutrino survival probability at the reactor neutrino oscillation.

The survival probability of $\bar{\nu}_e$ produced from reactors is

$$P_{\text{Th}}\left(\bar{\nu}_e \longrightarrow \bar{\nu}_e\right) = \left| \sum_{j=1}^{4} \left|\widetilde{U}_{ei}\right|^2 \exp i \frac{\Delta m_{j1}^2 L}{2E_\nu} \right|^2$$

$$= 1 - \sum_{i<j} 4\left|\widetilde{U}_{ei}\right|^2 \left|\widetilde{U}_{ej}\right|^2 \sin^2\left(\frac{\Delta m_{ij}^2 L}{4E_\nu}\right), \tag{3}$$

where Δm_{ij}^2 denotes the mass-squared difference $(m_i^2 - m_j^2)$. It can be expressed in terms of combined Δm_{ij}^2-driven oscillations as

$$P_{\text{Th}}\left(\bar{\nu}_e \longrightarrow \bar{\nu}_e\right) = 1 - c_{14}^4 c_{13}^4 \sin^2 2\theta_{12} \sin^2\left(1.27 \Delta m_{21}^2 \frac{L}{E}\right)$$

$$- c_{14}^4 \sin^2 2\theta_{13} \sin^2\left(1.27 \Delta m_{31}^2 \frac{L}{E}\right)$$

$$- c_{13}^2 \sin^2 2\theta_{14} \sin^2\left(1.27 \Delta m_{41}^2 \frac{L}{E}\right)$$

$$- s_{13}^2 \sin^2 2\theta_{14} \sin^2\left(1.27 \Delta m_{43}^2 \frac{L}{E}\right), \tag{4}$$

where $\Delta m_{32}^2 \approx \Delta m_{31}^2$ and $\Delta m_{42}^2 \approx \Delta m_{41}^2$. The size of m_4 relative to m_3 is not yet constrained. The above P_{Th} is understood only within a theoretical framework, since the energy of the detected neutrinos is not unique but is continuously distributed over a certain range. So, the observed quantity is established with a distribution of neutrino energy spectrum and an energy-dependent cross section. Analyses of neutrino oscillation average accessible energies of the neutrinos emerging from the reactors. The measured probability of survival is

$$\langle P \rangle = \frac{\int P_{\text{Th}}(E) \sigma_{\text{tot}}(E) \phi(E) \, dE}{\int \sigma_{\text{tot}}(E) \phi(E) \, dE}, \tag{5}$$

where $\sigma_{\text{tot}}(E)$ is the total cross-section of inverse beta decay (IBD), and $\phi(E)$ is the neutrino flux distribution from the reactor. The total cross section of IBD is given as

$$\sigma_{\text{tot}}(E) = 0.0952 \left(\frac{E_e \sqrt{E_e^2 - m_e^2}}{1\ \text{MeV}^2}\right) \times 10^{-42}\ \text{cm}^2, \tag{6}$$

where $E_e \approx E_\nu - (M_n - M_p)$ [28, 29]. The flux distribution $\phi(E)$ from the four isotopes (U^{235}, Pu^{239}, U^{238}, and Pu^{241}) at the reactors is expressed by the following exponential of a fifth order polynomials of E_ν:

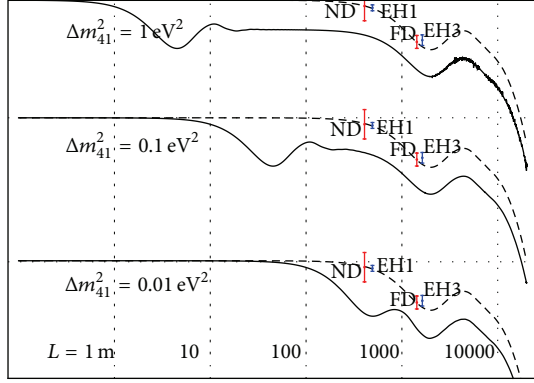$$\phi\left(E_\nu\right) = \exp\left(\sum_{i=0}^{5} f_i E_\nu^i\right), \tag{7}$$

FIGURE 1: The dependency of $\langle P \rangle$ in (5) on Δm^2_{41} is presented, when $\Delta m^2_{31} = 2.32 \times 10^{-3}$ eV^2 as taken in RENO and Daya Bay. Typical shapes of $\langle P \rangle$ versus distance are drawn for comparison with the measured ratios in the two experiments. The amplitudes of Δm^2_{31} oscillation and Δm^2_{41} oscillation are given by $\sin^2 2\theta_{13} = 0.10$ and $\sin^2 2\theta_{14} = 0.10$, respectively, as an example.

where $f_0 = +4.57491 \times 10$, $f_1 = -1.73774 \times 10^{-1}$, $f_2 = -9.10302 \times 10^{-2}$, $f_3 = -1.67220 \times 10^{-5}$, $f_4 = +1.72704 \times 10^{-5}$, and $f_5 = -1.01048 \times 10^{-7}$ are obtained by fitting the total flux of the four isotopes with the fission ratio expected at the middle of the reactor burn up period [30].

The curves in Figure 1 show $\langle P \rangle$ as L increases in a logarithmic manner, where the three patterns of probabilities are shown according to the order of Δm^2_{41}. The first bump in each curve corresponds to the oscillation due to Δm^2_{41}, while the second bump that appears near 1500 m corresponds to the oscillation due to Δm^2_{31}. RENO and Daya Bay were designed to observe the Δm^2_{31}-driven oscillations at far detector (FD) according to three-neutrino analysis, while additional detector(s) at a closer baseline performs the detection of neutrinos in the same condition. The comparison of the number of neutrino events at FD to the number of events at the near detector (ND) is an effective strategy to determine the disappearance of antineutrinos from reactors. That is, the $\sin^2 2\theta_{13}$ is evaluated by the slope of the curve between ND and FD, while their absolute values of event numbers do not affect the estimation of the angle θ_{13}. Both experiments used the normalization to adjust the data to satisfy the boundary condition which is that there is no oscillation effect before the ND. From Figure 1, it can be shown that the magnitude of Δm^2_{41} can affect not only the normalization factor but also the ratio between the FD and ND.

The six baselines of the near detector (ND) and the far detector (FD) of RENO are L_{near} (meters) = {660, 445, 302, 340, 520, 746} and L_{far} (meters) = {1560, 1460, 1400, 1380, 1410, 1480}, while their flux-weighted averages $\overline{L}_{\text{near}}$ and $\overline{L}_{\text{far}}$ are 407.3 m and 1443 m, respectively. The baselines of Daya Bay, named EH1, EH2, and EH3, have lengths of EH1 = 494 m, EH2 = 554 m, and EH3 = 1628 m, respectively, so that, conventionally, EH1 and EH2 are regarded as near detectors while EH3 is regarded as a far detector.

After the first release of results, Daya Bay and RENO updated the far-to-near ratio of neutrino events with additional data. Daya Bay reported a ratio of $R = 0.944 \pm 0.007$ (stat) ± 0.003 (syst) with $R(\text{EH1}) = 0.987 \pm 0.004$ (stat) ± 0.003 (syst) [31]. RENO also reported an update with additional data from March to October in 2012, where $R(\text{FD}) = 0.929 \pm 0.006$ (stat) ± 0.009 (syst) [26]. Their measurements are marked in Figure 1. In three-neutrino analysis, the far-to-near ratios give the Δm^2_{31}-oscillation amplitude $\sin^2 2\theta_{13} = 0.089 \pm 0.010$ (stat) ± 0.005 (syst) and $\sin^2 2\theta_{13} = 0.100 \pm 0.010$ (stat) ± 0.015 (syst) in Daya Bay and RENO, respectively. On the other hand, the far-to-near ratio and the measured-to-expected ratio are understood as a combination of Δm^2_{31} oscillations and Δm^2_{41} oscillations as shown in Figure 1. For a given value of Δm^2_{41}, 0.01 eV^2 or 0.01 eV^2, the combination of $\sin^2 2\theta_{14}$ and $\sin^2 2\theta_{13}$ is described in Figure 2. In the case of RENO, the $\langle P(\Delta m^2_{41} = 0.01 \text{ eV}^2) \rangle$ and $\langle P(\Delta m^2_{41} = 0.1 \text{ eV}^2) \rangle$ curves which pass the error bars at ND and FD are drawn as blue- (gray-) shaded areas. The area where the two shaded areas, ND and FD, overlap is the allowed region in $\sin^2 2\theta_{13} - \sin^2 2\theta_{14}$ space using rate-only analysis. The corresponding analysis for Daya Bay is shown together in Figure 2. The value of $\sin^2 2\theta_{13}$ is in good agreement with the results released by the two experiments.

3. Four-Neutrino Analysis of Updated Spectral Shape in RENO

One of RENO's results was the ratio of the observed to the expected number of antineutrinos in the far detector, $R = 0.929 \pm 0.011$ (see [26]), where the observed is simply the number of events at FD. On the other hand, the expected number of events at FD can be obtained using several adjustments of the number of events at ND:

$$R \equiv \frac{[\text{Observed at FD}]}{[\text{Expected at FD}]} \tag{8}$$

$$\equiv \frac{[\text{No. of events at FD}]}{[\text{No. of events at ND}]^*}, \tag{9}$$

where the number of events at each detector is normalized. The normalization of the neutrino fluxes at ND and FD requires an adjustment between the two individual detectors which includes corrections due to DAQ live time, detection efficiency, background rate, and the distance to each detector. The numbers of events at FD and ND in (9) have already been normalized by these correction factors, and so we have $R_{\text{far}} = 0.929 \pm 0.017$ and $R_{\text{near}} = 0.990 \pm 0.025$ as shown in Figure 2. The normalization guarantees $R = 1$ at the center of the reactors. RENO removes the oscillation effect at ND when evaluating the expected number of events at FD by dividing the denominator of (9) by 0.990 which is taken from R_{near}. Now,

$$R = \frac{[\text{No. of events at FD}]}{[\text{No. of events at ND}]/0.990}. \tag{10}$$
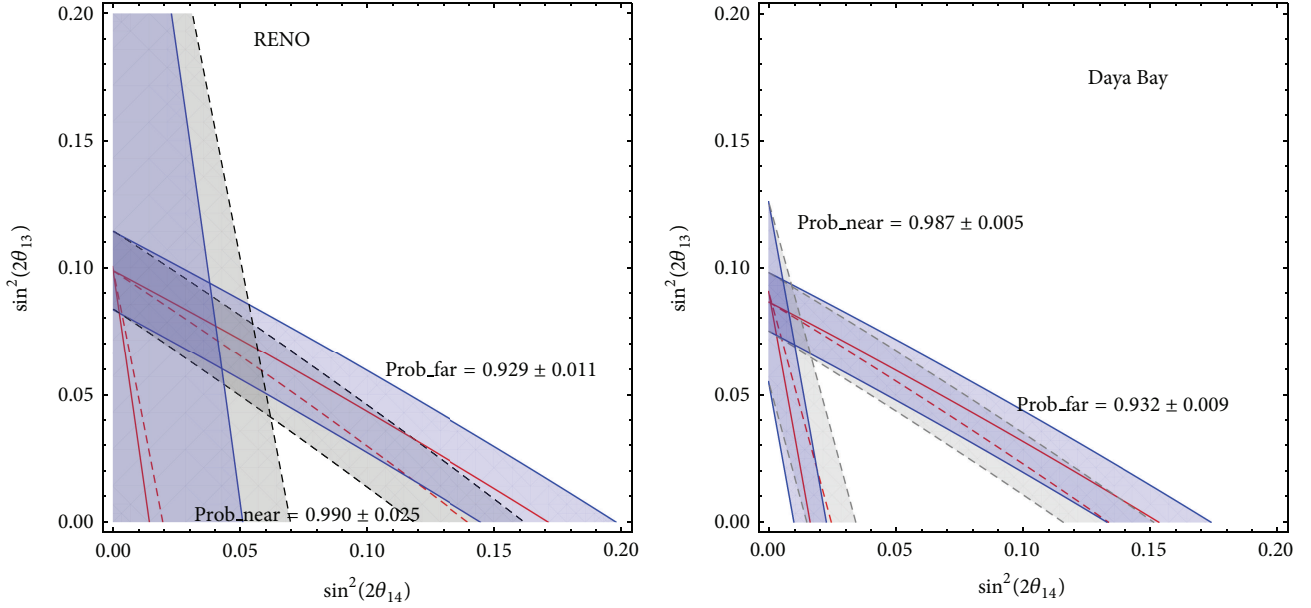
FIGURE 2: Four-neutrino analysis for the observed to expected ratios at both ND and FD of RENO. The shaded areas indicate the available combination of $\sin^2 2\theta_{13}$ and $\sin^2 2\theta_{14}$ which is compatible with the ranges of R_{Near} and R_{Far} released by RENO and Daya Bay. Blue (gray) areas are obtained with $\Delta m_{41}^2 = 0.01(0.1)\,\text{eV}^2$. The 4ν analysis of the far-to-near ratio at Daya Bay is also given for comparison.
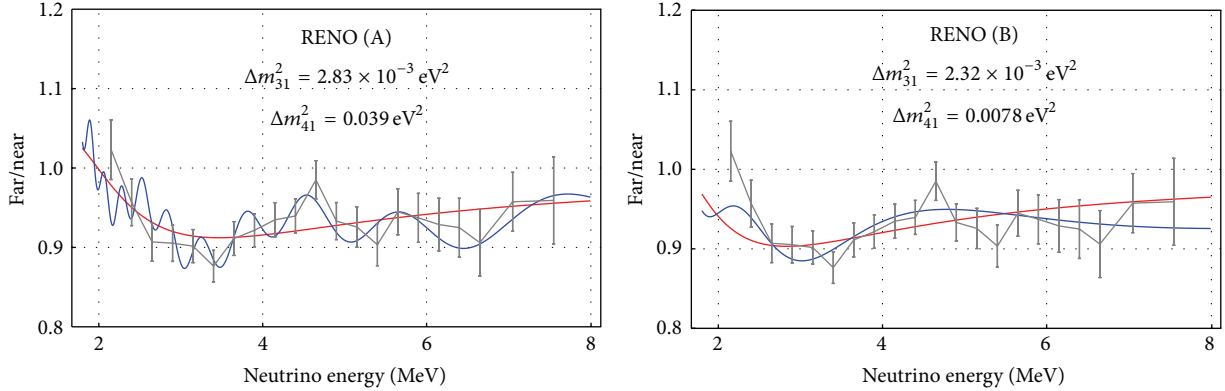

FIGURE 3: The data and error bars are the reproduction of updated RENO for an extended period until October 2012. The red fits are drawn with $\sin^2 2\theta_{14} = 0$ for $\Delta m_{31}^2 = 2.83 \times 10^{-3}\,\text{eV}^2$ and for $\Delta m_{31}^2 = 2.32 \times 10^{-3}\,\text{eV}^2$ obtained from the analysis in Figure 4. For each case, the blue fits are overlaid which are the superposition with $\Delta m_{41}^2 = 0.039\,\text{eV}^2$ oscillation of amplitude $\sin^2 2\theta_{14} = 0.050$, and the superposition with $\Delta m_{41}^2 = 0.0078\,\text{eV}^2$ oscillation of amplitude $\sin^2 2\theta_{14} = 0.054$, respectively, obtained from the analysis in Figure 5.

In rate-only analysis, the ratio of the observed to the expected number of events at FD in (8) is just the survival at FD, since the denominator in (10) is eliminated. Thus, R coincides with R_{far} in Figure 2.

In spectral shape analysis, however, the denominator cannot be neglected, since the oscillation effect at ND differs depending on the neutrino energy. The data points in Figure 3 are obtained by the definition of the ratio R given in (8) and (9) per 0.25 MeV bin, as the energy varies from 1.8 MeV to 12.8 MeV. The data dots and error bars were updated by including additional data from March to October in 2012 officially announced at Neutrino Telescope 2013 [26].

The ratio in (10) is compared with theoretical curves overlaid on the data points. The theoretical curves are described by

$$\frac{\langle P(\text{FD})\rangle}{\langle P(\text{ND})\rangle (0.990)^{-1}}, \quad (11)$$

where $\langle P(\text{L})\rangle$ is given in (4). In Figure 4, the best fit of $(\Delta m_{31}^2, \sin^2 2\theta_{13})$ is presented when $\theta_{14} = 0$. The point A $(0.00283\,\text{eV}^2, 0.09)$ indicates the χ^2 minimum where $\sin^2 2\theta_{13}$ and Δm_{31}^2 are parameters, while the point B $(0.00232\,\text{eV}^2, 0.10)$ is the minimum where Δm_{31}^2 is 0.00232
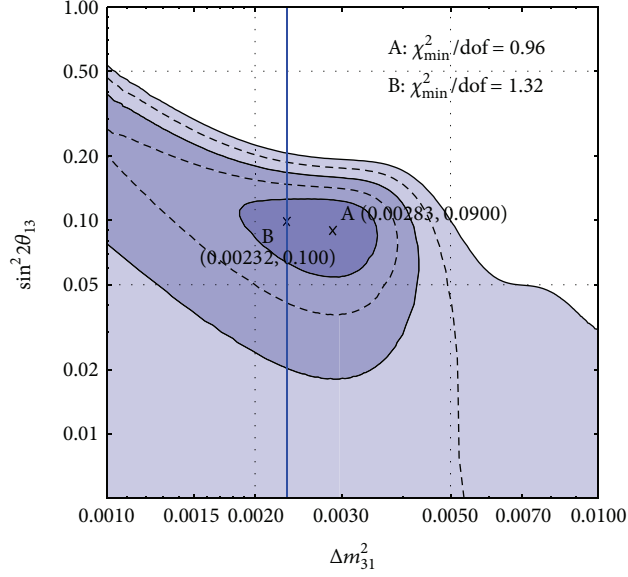
FIGURE 4: Three-neutrino analysis of the spectral shape updated until October 2012. The best fit in $(\Delta m_{31}^2, \sin^2 2\theta_{13})$ is (0.00283, 0.09) denoted by A. When $\Delta m_{31}^2 = 0.00232\,\text{eV}^2$ is fixed as taken by RENO, the best fit of $\sin^2\theta_{13}$ is 0.100. The 1σ, 2σ, and 3σ exclusion curves are drawn by solid lines.

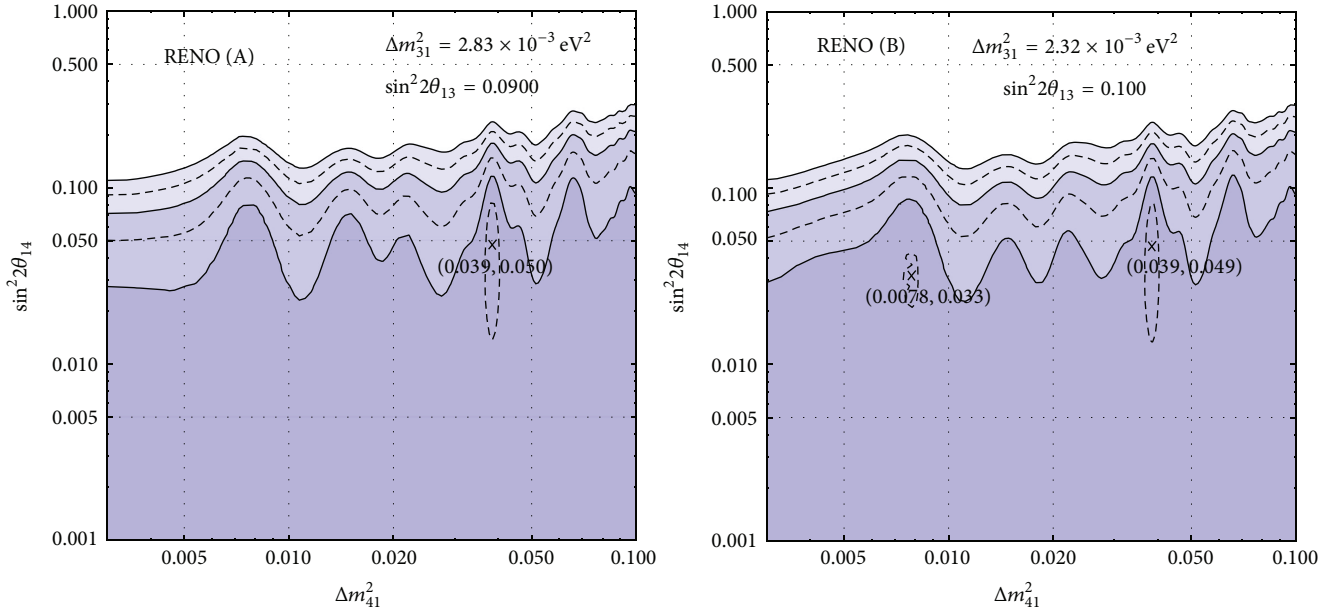FIGURE 5: The 1σ, 2σ, and 3σ exclusion curves are drawn by solid lines. Apparently, a broad range of $\sin^2 2\theta_{14}$ apparently remains not excluded. Only $\Delta m_{41}^2 > \Delta m_{31}^2$ is considered and $\sin^2 2\theta_{14} > 0.2$ is excluded at 3σ CL. For (A) specified by $\Delta m_{31}^2 = 2.83 \times 10^{-3}\,\text{eV}^2$, the minimum $\chi_{\min}^2/\text{dof} = 0.48$ is at $(\Delta m_{41}^2, \sin^2 2\theta_{14}) = (0.039\,\text{eV}^2, 0.050)$, while, for (B) specified by $\Delta m_{31}^2 = 2.32 \times 10^{-3}\,\text{eV}^2$, two minima $\chi_{\min}^2/\text{dof} = 1.06$ and 0.85 are located at $(\Delta m_{41}^2, \sin^2 2\theta_{14}) = (0.0078\,\text{eV}^2, 0.033)$ and $(0.039\,\text{eV}^2, 0.049)$, respectively.

which RENO and Daya Bay used for the fixed value. Hereafter, two cases depending on Δm_{31}^2 are discussed: one is for $\Delta m_{31}^2 = 0.00283\,\text{eV}^2$ marked by A and the other is for $\Delta m_{31}^2 = 0.00232\,\text{eV}^2$ marked by B. According to the analysis performed with $\theta_{14} = 0$, the red curves for the two values of Δ_{31}^2 are overlaid on the spectral data in Figure 3. Figure 5

shows interpretation of the spectral shape in terms of fourneutrino oscillation. For given values of Δ_{31}^2 and $\sin^2 2\theta_{13}$, the 1, 2, 3σ CL exclusion curves are obtained by convolution with the energy resolution of RENO detectors $(5.9/\sqrt{E} + 1.1)\%$. Using the best fits $(\Delta m_{41}^2, \sin^2 2\theta_{14}) = (0.039\,\text{eV}^2, 0.05)$ for (A) and $(\Delta m_{41}^2, \sin^2 2\theta_{14}) = (0.0078\,\text{eV}^2, 0.033)$ for (B),
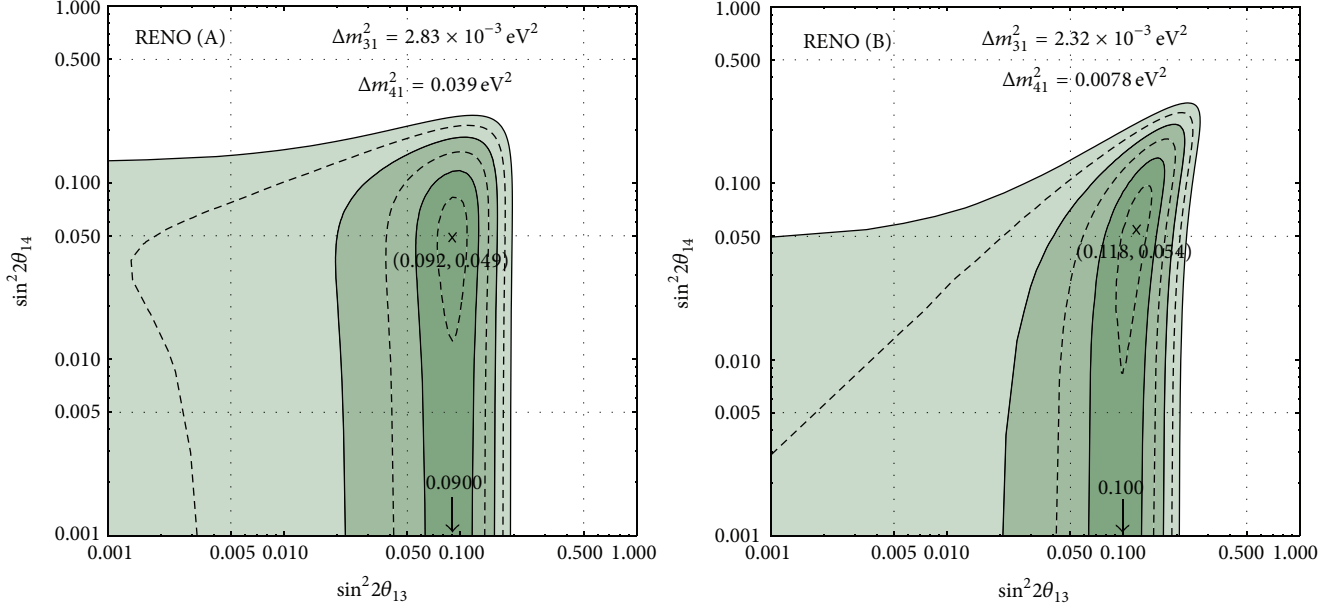
FIGURE 6: The 1σ, 2σ, and 3σ fit of combination of the $\sin^2 2\theta_{13}$ and $\sin^2 2\theta_{14}$ for chosen values of (Δm^2_{31} and Δm^2_{41}). For (A), the $\chi^2_{\min}$/dof of (0.092, 0.049) is 0.51. For (B), the $\chi^2_{\min}$/dof of (0.118, 0.049) is 0.96. In both cases, the best fit of $\sin^2 2\theta_{14} = 0$ is included in 1σ region.

the blue curves are also added on the spectral data in Figure 3. To see a distinct different aspect due to the magnitude of Δm^2_{41}, we choose $m^2_{41} = 0.0078\,\mathrm{eV}^2$ for the best fit of (B), avoiding $m^2_{41} = 0.039\,\mathrm{eV}^2$ which is the same as the m^2_{41} for (A).

The solid curves in Figure 6 explain 1σ, 2σ, and 3σ CL of $\Delta\chi^2$ in parameters ($\sin^2 2\theta_{13}$, $\sin^2 2\theta_{14}$), of which the best-fits are found at (0.092, 0.049) for case (A) of $\Delta m^2_{31} = 0.00283\,\mathrm{eV}^2$ and at (0.118, 0.054) for case (B) of $\Delta m^2_{31} = 0.00232\,\mathrm{eV}^2$. In case (B) where the value of Δm^2_{31} is the same as the one that RENO and Daya Bay took for it, the best fit of $\sin^2 2\theta_{13}$ is 0.118 in company with nonzero $\sin^2 2\theta_{14}$. The best fit $\sin^2 2\theta_{13} = 0.100$ with the restriction $\sin^2 2\theta_{14} = 0$ is still within 1σ region of four-neutrino analysis. Also in case (B) which is specified by a rather large Δm^2_{31} compared to the value taken by RENO and Daya Bay or the value suggested by global analyses, the best fit $\sin^2 2\theta_{13} = 0.090$ of three-neutrino analysis is placed in the region of 1σ CL. This implies no preference between three-neutrino and four-neutrino schemes when the shape in Figure 3 is analyzed in this rough estimation.

4. Conclusion

If a fourth type of neutrino has a mass not much larger than the other three masses, the results of reactor neutrino oscillations like RENO, Daya Bay, and Double Chooz can be affected by the fourth state. For detectors established for oscillations driven by $\Delta m^2_{31} = 0.00232\,\mathrm{eV}^2$, clues about the fourth neutrino can be perceived only if the order of Δm^2_{41} is not much larger than that of Δm^2_{31}. Therefore, this work examined the possibility of a kind of sterile neutrino in the range of mass-squared differences below $0.1\,\mathrm{eV}^2$,

considering the two announced results of RENO and Daya Bay. Anomalies of reactor antineutrino oscillations have been considered for the range, $0.1\,\mathrm{eV}^2 < \Delta m^2_{14} < 1\,\mathrm{eV}^2$. Thus, it is worth analyzing the absolute flux at the near detector and the ratio of the far-to-near flux on a common basis [32].

RENO announced an update of rate-only analysis and the spectral shape of neutrino events [neutrino telescope], including an observed-to-expected ratio $R = 0.929$ and an oscillation amplitude of $\sin^2 2\theta_{13} = 0.100$. We compared the spectral shape with theoretical curves of the superpositions of Δm^2_{41} oscillations and Δm^2_{31} oscillations. In summary, $\sin^2 2\theta_{14} > 0.2$ is excluded at 3σ CL. When $\Delta m^2_{31} = 0.00232\,\mathrm{eV}^2$ is fixed, the best-fit in four-neutrino parameters is (Δm^2_{41}, $\sin^2 2\theta_{14}$) = (0.0078 eV², 0.054). When we search the fit of Δm^2_{31} along with other parameters of four-neutrino analysis, the best value is obtained $\Delta m^2_{31} = 0.00283\,\mathrm{eV}^2$ with $\sin^2 2\theta_{13} = 0.090$ from the shape in three-neutrino analysis. When the parameters are extended to four-neutrino scheme, the best fit is (Δm^2_{41}, $\sin^2 2\theta_{14}$) = (0.039 eV², 0.049). As shown in Figure 6, the three-neutrino analysis of RENO ($\sin^2 2\theta_{13}$, $\sin^2 2\theta_{14}$) = (0.100, 0.0) is also included within 1σ CL in four-neutrino analysis. Thus, it is not yet known whether the superposition with Δm^2_{41} oscillations is preferred to the single Δm^2_{31} oscillations at RENO detectors. Figure 7 shows that the rate-only analysis and the spectral shape analysis are in good agreement within their 1σ CL range.
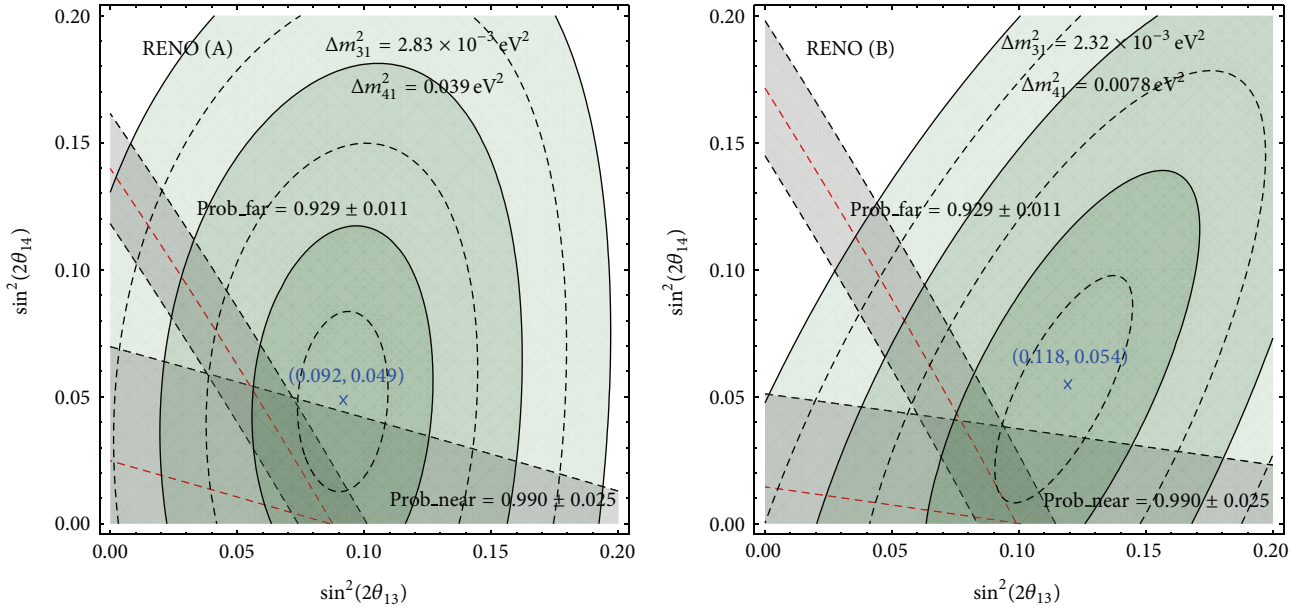
FIGURE 7: Comparison of rate-only analysis and spectral shape analysis: in both (A) and (B), the regions allowed by rate-only analysis are overlapped in 1σ range of shape analysis, while they do not include the χ^2-minimum best fits.

References

[1] Z. Maki, M. Nakagawa, and S. Sakata, "Remarks on the unified model of elementary particles," *Progress of Theoretical Physics*, vol. 28, no. 5, pp. 870–880, 1962.

[2] F. P. An, J. Z. Bai, A. B. Balantekin et al., "Observation of electron-antineutrino disappearance at daya bay," *Physical Review Letters*, vol. 108, no. 17, Article ID 171803, 7 pages, 2012.

[3] J. K. Ahn, S. Chebotaryov, J. H. Choi et al., "Observation of reactor electron antineutrinos disappearance in the RENO experiment," *Physical Review Letters*, vol. 108, no. 19, Article ID 191802, 6 pages, 2012.

[4] K. Abe, N. Abgrall, Y. Ajima et al., "Indication of electron neutrino appearance from an accelerator-produced off-axis muon neutrino beam," *Physical Review Letters*, vol. 107, no. 4, Article ID 041801, 8 pages, 2011.

[5] P. Adamson, D. J. Auty, D. S. Ayres et al., "Improved search for muon-neutrino to electron-neutrino oscillations in MINOS," *Physical Review Letters*, vol. 107, no. 18, Article ID 181802, 6 pages, 2011.

[6] Y. Abe, C. Aberle, T. Akiri et al., "Indication of reactor $\overline{\nu}_e$ disappearance in the double chooz experiment," *Physical Review Letters*, vol. 108, no. 13, Article ID 131801, 7 pages, 2012.

[7] Y. Abe, C. Aberle, J. C. Anjos et al., "Reactor electron antineutrino disappearance in the Double Chooz experiment," *Physical Review D*, vol. 86, no. 5, Article ID 052008, pp. 1–21, 2012.

[8] J. Beringer, J. F. Arguin, R. M. Barnett1 et al., "Review of particle physics," *Physical Review D*, vol. 86, no. 1, Article ID 010001, 2012.

[9] G. L. Fogli, E. Lisi, A. Marrone, D. Montanino, A. Palazzo, and A. M. Rotunno, "Solar neutrino oscillation parameters after first KamLAND results," *Physical Review D*, vol. 67, no. 7, Article ID 073002, 2003.

[10] D. V. Forero, M. Tortola, and J. W. F. Valle, "Global status of neutrino oscillation parameters after Neutrino-2012," *Physical Review D*, vol. 86, no. 7, Article ID 073012, 8 pages, 2012.

[11] M. C. Gonzalez-Garcia, M. Maltoni, J. Salvado, and T. Schwetz, "Global fit to three neutrino mixing: critical look at present precision," *Journal of High Energy Physics*, vol. 2012, article 123, 2012.

[12] A. Aguilar-Arevalo, L. B. Auerbach, R. L. Burman et al., "Evidence for neutrino oscillations from the observation of anti-neutrino(electron) appearance in a anti-neutrino(muon) beam," *Physical Review D*, vol. 64, no. 11, Article ID 112007, 22 pages, 2001.

[13] A. A. Aguilar-Arevalo, A. O. Bazarko, and S. J. Brice, "Search for electron neutrino appearance at the $\triangle m^2 \sim 1\,eV^2$ Scale," *Physical Review Letters*, vol. 98, no. 23, Article ID 231801, 7 pages, 2007.

[14] A. A. Aguilar-Arevalo, C. E. Anderson, S. J. Brice et al., "Event excess in the miniBooNE search for $\overline{\nu}_\mu \rightarrow \overline{\nu}_e$ oscillations," *Physical Review Letters*, vol. 105, no. 18, Article ID 181801, 5 pages, 2010.

[15] A. A. Aguilar-Arevalo et al., "Improved search for $\overline{\nu}_\mu \rightarrow \overline{\nu}_e$ Oscillations in the miniBooNE experiment," *Physical Review Letters*, vol. 110, article 16, Article ID 181801, 6 pages, 2010.

[16] W. Hampel, J. Handt, G. Heusser et al., "GALLEX solar neutrino observations: results for GALLEX IV," *Physics Letters B*, vol. 447, no. 1-2, pp. 127–133, 1999.

[17] J. N. Abdurashitov, T. J. Bowles, C. Cattadori et al., "The BNO-LNGS joint measurement of the solar neutrino capture rate in71Ga," *Astroparticle Physics*, vol. 25, no. 5, pp. 349–354, 2006.

[18] B. Achkar, R. Aleksan, M. Avenier et al., "Search for neutrino oscillations at 15, 40 and 95 meters from a nuclear power reactor at Bugey," *Nuclear Physics B*, vol. 434, no. 3, pp. 503–532, 1995.

[19] S. K. Kang, Y. D. Kim, Y. Ko, and K. Siyeon, "Sterile neutrino analysis of reactor-neutrino oscillation," http://arxiv.org/abs/1303.6173.

[20] K. Bora, D. Dutta, and P. Ghoshal, "Probing sterile neutrino parameters with Double Chooz, Daya Bay and RENO," *Journal of High Energy Physics*, vol. 2012, article 25, 2012.

[21] Y. Gao and D. Marfatia, "Meter-baseline tests of sterile neutrinos at Daya Bay," *Physics Letters B*, vol. 723, no. 1-3, pp. 164–167, 2013.

[22] C. Giunti, M. Laveder, Y. F. Li, Q. Y. Liu, and H. W. Long, "Update of short-baseline electron neutrino and antineutrino disappearance," *Physical Review D*, vol. 86, no. 11, Article ID 113014, 14 pages, 2012.

[23] J. M. Conrad, C. M. Ignarra, G. Karagiorgi, M. H. Shaevitz, and J. Spitz, "Sterile neutrino fits to short-baseline neutrino oscillation measurements," *Advances in High Energy Physics*, vol. 2013, Article ID 163897, 26 pages, 2013.

[24] S. N. Gninenko, "Sterile neutrino decay as a common origin for LSND/MiniBooNE and T2K excess events," *Physical Review D*, vol. 85, no. 5, Article ID 051702, 5 pages, 2012.

[25] J. Kopp, P. A. N. Machado, M. Maltoni, and T. Schwetz, "Sterile neutrino oscillations: the global picture," *Journal of High Energy Physics*, vol. 2013, article 50, 2013.

[26] S. H. Seo, "New results from RENO," in *Proceedings of the 15th International Workshop on Neutrino Telescopes*, Venice, Italy, March 2013.

[27] G. Mention, M. Fechner, T. Lasserre et al., "Reactor antineutrino anomaly," *Physical Review D*, vol. 83, no. 7, Article ID 073006, 2011.

[28] T. A. Mueller, D. Lhuillier, M. Fallot et al., "Improved predictions of reactor antineutrino spectra," *Physical Review C*, vol. 83, no. 5, Article ID 054615, 2011.

[29] P. Vogel and J. F. Beacom, "Angular distribution of neutron inverse beta decay, $\bar{\nu}_e + \vec{p}e^+ + n$," *Physical Review D*, vol. 60, no. 5, Article ID 053003, 1999.

[30] P. Huber, "Determination of antineutrino spectra from nuclear reactors," *Physical Review C*, vol. 84, no. 2, Article ID 024617, 16 pages, 2012, Erratum in *Physical Review C*, vol. 85, no. 2, Article ID 029901, 2012.

[31] F. P. An, Q. An, J. Z. Bai et al., "Improved measurement of electron antineutrino disappearance at Daya Bay," *Chinese Physics C*, vol. 37, no. 1, Article ID 011001, 2013.

[32] RENO Collaboration, "Absolute flux of reactor antineutrinos," in preparation.